

12

INVESTIGATION OF THE RAYLEIGH CRITICAL ANGLE PHENOMENON  
FOR THE CHARACTERIZATION OF SURFACE PROPERTIES  
PHASE II

AD A1 25050

A TECHNICAL REPORT

30 December 1982

DTIC  
FEB 28 1983  
H

Prepared For:

Air Force Office of Scientific Research  
Bolling Air Force Base  
Washington, D.C. 20332

**S**PECTRON  
**S**DEVELOPMENT  
**L**ABORATORIES  
INC.

Approved for public release  
distribution unlimited.

83 02 028 077

DTIC FILE COPY

12

INVESTIGATION OF THE RAYLEIGH CRITICAL ANGLE PHENOMENON  
FOR THE CHARACTERIZATION OF SURFACE PROPERTIES  
PHASE II

A TECHNICAL REPORT  
30 December 1982  
SDL No. 83-2188-13TR

Principal Investigator  
B. P. Hildebrand  
  
Senior Scientist  
G. L. Fitzpatrick  
  
Computer Scientist  
A. J. Boland

DTIC  
FEB 28 1983  
H

Sponsored by:

Advanced Research Projects Agency (DOD)  
ARPA Order No. 4109  
Monitored by AFOSR under Contract #F49620-81-C-0040

"The views and conclusions contained in this document are those of the authors and should not be interpreted as necessarily representing the official policies, either expressed or implied, of the Defense Advanced Research Projects Agency of the U.S. Government."

**S**PECTRON  
**D**EVELOPMENT  
**L**ABORATORIES  
INC.

DEFENSE OFFICE OF SCIENTIFIC RESEARCH (AFSC)  
NOTICE OF... DTIC  
This technical report was prepared and is  
approved for distribution under AFM 193-12.  
Distribution is unlimited.  
MATTHEW J. KERNER  
Chief, Technical Information Division

Seattle Laboratory: 1010 Industry Drive  
Seattle, Washington 98188 (206) 575-9324

## TABLE OF CONTENTS

<u>No.</u>		<u>Page</u>
	TABLE OF CONTENTS . . . . .	i
	LIST OF FIGURES . . . . .	ii
	REPORT DOCUMENTATION PAGE . . . . .	iii
1.0	INTRODUCTION . . . . .	1
2.0	CRITICAL ANGLE MEASUREMENTS . . . . .	4
3.0	EXPERIMENTS . . . . .	8
4.0	SPECTRAL MEASUREMENTS . . . . .	23
5.0	SUMMARY . . . . .	27
6.0	ACKNOWLEDGMENTS . . . . .	28
7.0	REFERENCES . . . . .	29

Classification For

Page 01.A1

Page 02B

Page 03C

Distribution

---


Distribution/

Availability Codes

Avail and/or

Dist Special

A



## LIST OF FIGURES

<u>No.</u>		<u>Page</u>
1	Focused acoustic source and point receiver combination used in experiments . . . . .	5
2	Critical angles ( $\theta$ ) vs $\phi$ for a 4340 steel sample . .	9
3	Rotation of samples . . . . .	10
4	The x, y and z axes of a quartz crystal . . . . .	11
5	Critical angles ( $\theta$ ) vs $\phi$ for an x-cut quartz specimen . . . . .	13
6	Critical angles ( $\theta$ ) vs $\phi$ for a y-cut quartz specimen . . . . .	14
7	Critical angles ( $\theta$ ) vs $\phi$ for a silicon single crystal . . . . .	15
8	Miller indices for cubic crystals . . . . .	16
9	Critical angles ( $\theta$ ) vs $\phi$ for an aluminum single crystal . . . . .	18
10	Critical angles ( $\theta$ ) vs $\phi$ for a spinel single crystal . . . . .	19
11	Critical angles ( $\theta$ ) vs $\phi$ for a single crystal of lithium niobate . . . . .	20
12	This figure illustrates critical angle measurements on five specimens of a titanium alloy with varying O <sub>2</sub> content . . . . .	21
13	This figure illustrates fundamental and second harmonic amplitudes present in the reflected signal from an isotropic specimen of optical glass at and near the Rayleigh critical angle . . . . .	26

UNCLASSIFIED

SECURITY CLASSIFICATION OF THIS PAGE (When Data Entered)

REPORT DOCUMENTATION PAGE		READ INSTRUCTIONS BEFORE COMPLETING FORM
1. REPORT NUMBER <del>AFOSR</del> TR- 82-1093	2. GOVT ACCESSION NO. 40-4125 050	3. RECIPIENT'S CATALOG NUMBER
4. TITLE (and Subtitle) INVESTIGATION OF THE RAYLEIGH CRITICAL ANGLE PHENOMENON FOR THE CHARACTERIZATION OF SURFACE PROPERTIES, PHASE II	5. TYPE OF REPORT & PERIOD COVERED Quarterly R&D Status Report (Sept.-Nov. 1982)	
	6. PERFORMING ORG. REPORT NUMBER	
7. AUTHOR(s) B. P. Hildebrand, G. L. Fitzpatrick, and A. J. Boland	8. CONTRACT OR GRANT NUMBER(s) F49620-81-C-0040	
9. PERFORMING ORGANIZATION NAME AND ADDRESS Spectron Development Laboratories, Inc. Seattle Laboratory 1010 Industry Dr. Seattle, WA 98188	10. PROGRAM ELEMENT, PROJECT, TASK AREA & WORK UNIT NUMBERS 61102F 2306A2	
11. CONTROLLING OFFICE NAME AND ADDRESS Air Force Office of Scientific Research/NE Bldg. 410 Bolling Air Force Base Washington, D.C. 20332	12. REPORT DATE December 30, 1982	
	13. NUMBER OF PAGES 29	
14. MONITORING AGENCY NAME & ADDRESS (if different from Controlling Office)	15. SECURITY CLASS. (of this report) Unclassified	
	15a. DECLASSIFICATION/DOWNGRADING SCHEDULE	
16. DISTRIBUTION STATEMENT (of this Report)  Approved for public release; distribution unlimited.		
17. DISTRIBUTION STATEMENT (of the abstract entered in Block 20, if different from Report)		
18. SUPPLEMENTARY NOTES		
19. KEY WORDS (Continue on reverse side if necessary and identify by block number) Rayleigh critical angle      Third order elastic constants Rayleigh waves                Higher harmonics Surface waves                   Anisotropy Pseudosurface waves Nonlinear effects		
20. ABSTRACT (Continue on reverse side if necessary and identify by block number) Rayleigh critical angle experiments (on a water-solid interface) have been performed on samples ranging from single crystals to polycrystalline alloys and glasses. Two basic conclusions can be drawn from this work: 1) linear equations of motion (which include anisotropy) suffice for an approximate description of the observations, including the calculation of critical angles from second order elastic constants; 2) at and near the Rayleigh critical angle, anomalous production of harmonics is observed. This strongly implies		

DD FORM 1 JAN 73 1473 EDITION OF 1 NOV 68 IS OBSOLETE

UNCLASSIFIED SECURITY CLASSIFICATION PAGE (When Data Entered)

**UNCLASSIFIED**

SECURITY CLASSIFICATION OF THIS PAGE(When Data Entered)

20. that the nonlinear characteristics of the solid (which involves third order elastic constants) cannot be ignored in a complete description of the Rayleigh critical angle phenomenon.

Other explanations for these effects involving the nonlinear properties of water cannot yet be excluded. Accordingly, further spectral response measurements of a more precise and absolute nature are being pursued. Such measurements should provide a complete characterization of the phenomenon including the separate roles played by the water path and the solid.

**UNCLASSIFIED**

SECURITY CLASSIFICATION OF THIS PAGE(When Data Entered)

## 1.0 INTRODUCTION

In the last quarterly report (30 September 1982), we described a number of interesting critical angle experiments on z-cut quartz, optical glass, and a copper single crystal. In the present report, we document results of additional measurements on other materials and crystals including:

Quartz (x,y-cut crystals)  
Silicon Single Crystal  
Aluminum Single Crystal  
Lithium Niobate Single Crystal  
Spinel Single Crystal  
4340 Steel Sample (polycrystalline)  
Titanium Alloy (5 samples with  
varying O<sub>2</sub> content)(polycrystalline).

In general, these experiments demonstrate that linear equations of motion describe the gross features of the data, provided we also take anisotropy into account. That is, the relevant equation of motion is Newton's second law (Einstein notation)

$$\rho \ddot{U}_i = \partial \sigma_{ik} / \partial X_k \quad (1)$$

where the stress tensor  $\sigma_{ik} = \lambda_{iklm} U_{lm}$  depends on the adiabatic moduli of elasticity  $\lambda_{iklm}$ , and the strain

$$U_{lm} = \frac{1}{2} \left( \frac{\partial U_l}{\partial X_m} + \frac{\partial U_m}{\partial X_l} + \frac{\partial U_r}{\partial X_l} \frac{\partial U_r}{\partial X_m} \right) \quad (2)$$

In the linear approximation, higher order strains are dropped, and

$$U_{lm} \approx \frac{1}{2} \left( \frac{\partial U_l}{\partial X_m} + \frac{\partial U_m}{\partial X_l} \right) \quad (3)$$

is substituted into Eq. (1) to yield an equation of motion for linear anisotropic media<sup>1</sup>

$$\rho \ddot{u}_i = \lambda_{ik\ell m} \frac{\partial^2 u_m}{\partial x_k \partial x_\ell} \quad (4)$$

This equation has monochromatic bulk wave solutions

$$u_i = U_{0i} e^{i(\bar{k} \cdot \bar{r} - \omega t)} \quad (5)$$

where the wavevector  $\bar{k}$  is a function of frequency  $\omega$  satisfying Eq. (4). Substitution of Eq. (5) into Eq. (4)

$$(\rho \omega^2 \delta_{im} - \lambda_{ik\ell m} k_k k_\ell) U_m = 0 \quad (6)$$

yields three homogeneous equations in the unknown particle displacements

$$U_1 = U_x, \quad U_2 = U_y \quad \text{and} \quad U_3 = U_z \quad .$$

Nontrivial solutions of Eq. (6) require that the determinant of the coefficients vanish yielding the cubic equation in  $\omega^2$

$$|\lambda_{ik\ell m} k_k k_\ell - \rho \omega^2 \delta_{im}| = 0. \quad (7)$$

Thus, there are, in general, three bulk wave velocities in any linear anisotropic solid. When these considerations are extended to a water - (anisotropic linear solid) boundary,<sup>2</sup> it is found not only that critical angles vary as a function of the angle of rotation of the solid, but also may be multiple. That is, two surface wave critical angles sometimes exist.

All crystals, some alloys, and a variety of other materials exhibit anisotropic elastic properties. Observations and theory are in good agreement with linear elasticity theory (see above) in the sense that the multiple critical angles appear where predicted and with the proper magnitude.



However, a variety of other experimental observations (see previous reports) apparently involve more than the simple linear theory for their explanation. For example, the overall measuring process involves a water path, and water is a relatively nonlinear substance in comparison to most solids.<sup>3</sup> Moreover, there are indications,<sup>4</sup> that at and near the critical angle, the sample may also exhibit nonlinear behavior.

## 2.0 CRITICAL ANGLE MEASUREMENTS

In addition to two bulk wave solutions in an isotropic solid, there are surface wave solutions on a free surface which propagate at the velocity  $C_R$  given by

$$C_R = C_T \eta \quad (8)$$

where  $\eta$  is the single root of the Rayleigh characteristic equation<sup>5</sup>

$$\eta^6 - 8\eta^4 + 8\eta^2 \left( 3 - 2 \frac{C_T^2}{C_L^2} \right) - 16 \left( 1 - \frac{C_T^2}{C_L^2} \right) = 0$$

having the value  $|\eta| < 1$ . This is given approximately by

$$\eta_R = \frac{.87 + 1.12\sigma}{1 + \sigma} \quad (9)$$

Here,  $C_T$  and  $C_L$  are, respectively, the transverse and longitudinal velocities and  $\sigma$  is Poisson's ratio. These waves are the so-called Rayleigh waves that propagate on a vacuum-solid interface. They are characterized by a rapid reduction in amplitude as a function of distance from the boundary and penetrate roughly one wavelength below the solid surface.

Even with liquid loading, the surface waves propagate along the liquid-solid interface with essentially the same velocity  $C_R$ .<sup>2</sup> However, when liquid loading is present, a new and very useful feature enters as illustrated in Fig. 1. The propagating surface waves "leak" back into the water, combine, and interfere with the specularly reflected wave.

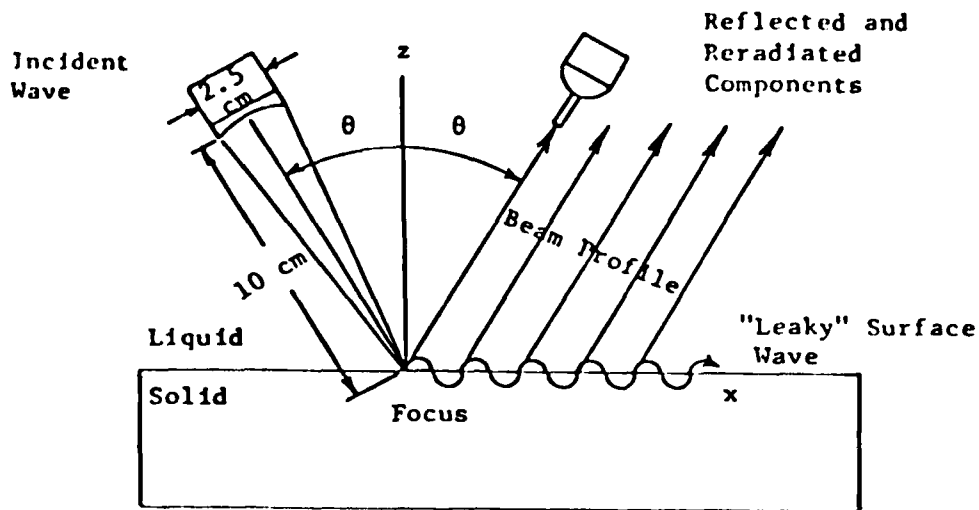


Fig. 1. Focused acoustic source and point receiver combination used in experiments. The source has an aperture of 2.54 cm and a 10 cm focal length. The transducer had a 5 MHz center frequency and is typically driven at 10 volts peak-to-peak (at various frequencies 1-10 MHz). Amplitudes recorded by the point detector are typically in the 1 volt range away from the critical angle while they are typically in the millivolt range at the critical angle.

Various investigators have studied the resultant nonspecular reflection field obtaining expressions for the reflection coefficient under various conditions.<sup>6,7</sup> In general, the reflection coefficient for a spatially unbounded beam may be written following Richardson<sup>7</sup> as

$$R = \frac{\cos^2 2\gamma_{22} + (c_{22}/c_{12})^2 \sin 2\gamma_{12} \sin 2\gamma_{22} + \rho_1 c_{11} \sin \gamma_{12} / \rho_2 c_{12} \sin \gamma_{11}}{\cos^2 2\gamma_{22} + (c_{22}/c_{12})^2 \sin 2\gamma_{12} \sin 2\gamma_{22} - \rho_1 c_{11} \sin \gamma_{12} / \rho_2 c_{12} \sin \gamma_{11}}, \quad (10)$$

where  $c_{12}$  = velocity of longitudinal waves in the solid,  
 $c_{22}$  = velocity of shear waves in the solid,  
 $c_{11}$  = velocity of longitudinal waves in the liquid,  
 $\theta = \gamma_{11}$  = angle of incidence of the longitudinal wave in the liquid,  
 $\gamma_{12}$  = angle of refracted longitudinal wave in the solid,  
 $\gamma_{22}$  = angle of refracted shear wave in the solid,  
 $\rho_1$  = density of liquid  
 $\rho_2$  = density of solid.

Angles are measured in the counterclockwise direction from the plane of the interface. The velocities are the complex quantities

$$c = v(1 + i\alpha/\omega), \quad (11)$$

$v$  = normal velocity,  
 $\alpha$  = attenuation,  
 $\omega$  = radian frequency.

The refracted angles are found by the generalized Snell's law,

$$\frac{\cos \gamma_{1j}}{c_{1j}} = h. \quad (12)$$

As discussed in previous reports, the reflection coefficient exhibits a sharp dip and a phase shift at the so-called Rayleigh critical angle  $\theta_R$  where ( $V_w$  = longitudinal wave velocity in water)

$$\sin\theta_R \approx \frac{V_w}{C_R} . \quad (13)$$

The above discussion applies to isotropic materials. When anisotropies are present, the problem is much more complex. As discussed in the September 30, 1982 quarterly report, Eq. (13) breaks down and the phenomenon of multiple surface wave critical angles occurs. In the following, we illustrate new results on both isotropic and anisotropic materials.

### 3.0 EXPERIMENTS

The results of measurements performed on a 4340 steel specimen are illustrated in Fig. 2. See Fig. 3 for a description of the angles involved. From Fig. 2 it might at first appear that the entire specimen is isotropic. That is, since the critical angle is close to  $\theta \approx 31.5^\circ$  for all orientations  $\phi$ , there would appear to be only two elastic constants ( $\lambda$  and  $\mu$  or  $E$  and  $\sigma$ ), and the equation of motion

$$\rho \ddot{\bar{U}} = \mu \nabla^2 \bar{U} + (\lambda + \mu) \nabla (\nabla \cdot \bar{U}) \quad (14)$$

would admit only one Rayleigh type surface wave solution.<sup>5</sup> Thus, only one Rayleigh type critical angle would be expected. Note, however, that these measurements characterize a region on the liquid-solid interface which measures roughly only one wavelength in water ( $\lambda \approx .04$  cm) in diameter.

We have found other regions on this same specimen (not illustrated, but see April 1982 Final Report) that are highly anisotropic and exhibit more than one critical angle. This observation illustrates in a dramatic fashion how the focused lens source and point receiver combination allow us to "map" or "image" the local elastic properties at different points on a surface.

Next we turn to an examination of x and y cuts of crystalline quartz (see Fig. 4 and Table I). In Figs. 5 and 6, we illustrate radial plots of the measured critical angles. Note that the z direction is encountered in rotating both x and y cuts about an axis normal to their surfaces, and as expected, the critical angle measured along z is the same for both cuts (see Figs. 5 and 6).

Figure 7 illustrates data taken on an unoriented single crystal of silicon. This illustrates the ability of the measurement system to orient such a crystal. Since silicon is cubic (see Fig. 8), rotation about the (111) axis would be expected to produce critical

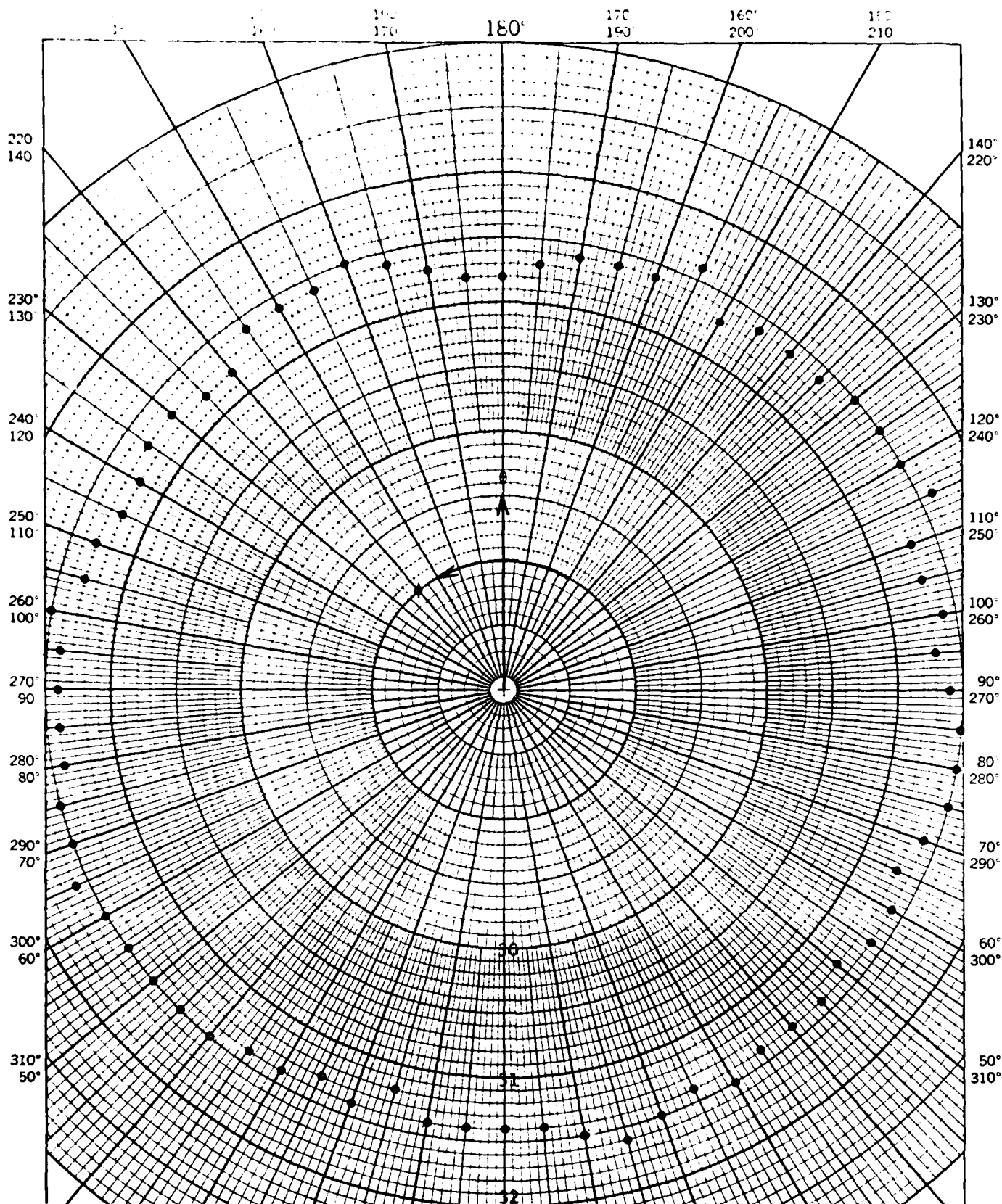


Fig. 2. Critical angles ( $\theta$ ) vs  $\phi$  for a 4340 steel sample. The frequency was 4.1 MHz, temperature 20°C, and source oscillator amplitude 6.5 volts. The material appears to be approximately isotropic in the small region of measurement (the lens focus).

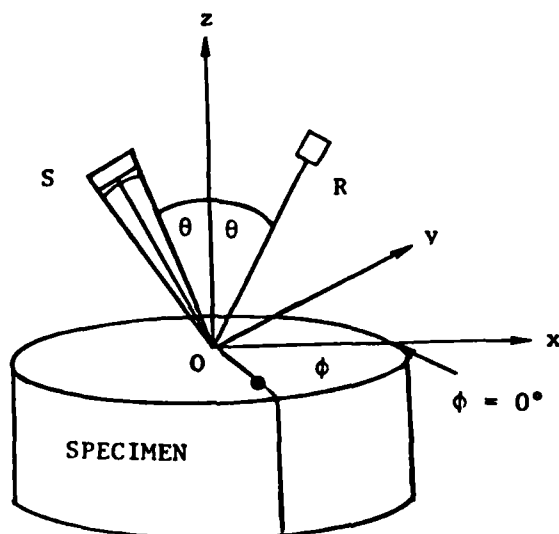


Fig. 3. Rotation of Samples. Samples are arbitrarily marked with a spot as shown. The spot is located along the positive x-axis which initially lies in the incident plane (S-O-R) of the source and receiver. The normal to the specimen surface lies along the z-axis for all azimuthal angles  $\phi$ . We arbitrarily label the x direction  $\phi = 0^\circ$  and turn the specimen counterclockwise.



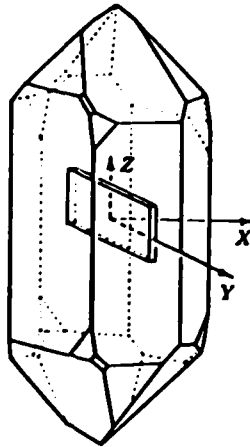


Fig. 4. The x, y and z axes of a quartz crystal. An x-cut slab (perpendicular to x axis) is illustrated. A z-cut slab would be perpendicular to the z axis which is also the symmetry axis of the crystal. Note that the x axis penetrates the line of intersection of two vertical faces of the crystal while the y axis is perpendicular to these faces. The x and y axes are at  $90^\circ$  to one another and to the z axis.

TABLE I Experimental Materials (Crystals)

Name	Crystal System	Description	Orientation
Silicon (Si)	Cubic	Disk: 3.2 cm dia, .9 cm thick	
Quartz (SiO <sub>2</sub> )	Hexagonal	Disk: 2.5 cm dia, 1.3 cm thick	(x,y,z-cuts)
Lithium Niobate (LiNbO <sub>3</sub> )	Hexagonal	Disk: 3 cm dia, .75 cm thick	
Spinel (MgAl <sub>2</sub> O <sub>4</sub> )	Cubic	Rod: 2.8 cm dia, 2.5 cm long	
Sapphire (Al <sub>2</sub> O <sub>3</sub> )	Hexagonal	Disk: 5 cm dia, .35 cm thick	
Copper (Cu)	Cubic	Rod: 2.5 cm dia, 1.9 cm long	(100)
Aluminum (Al)	Cubic	Rod: 2.54 cm dia 2.54 cm long	(100)
Lead (Pb)	Cubic	Rod: 2.54 cm dia, 2.8 cm long	(100)
Silver (Ag)	Cubic	Disk: 1.5 cm dia, .6 cm thick	
Iron (Fe)	Cubic	Rod: 1.0 cm dia, 2.5 cm long	(110)

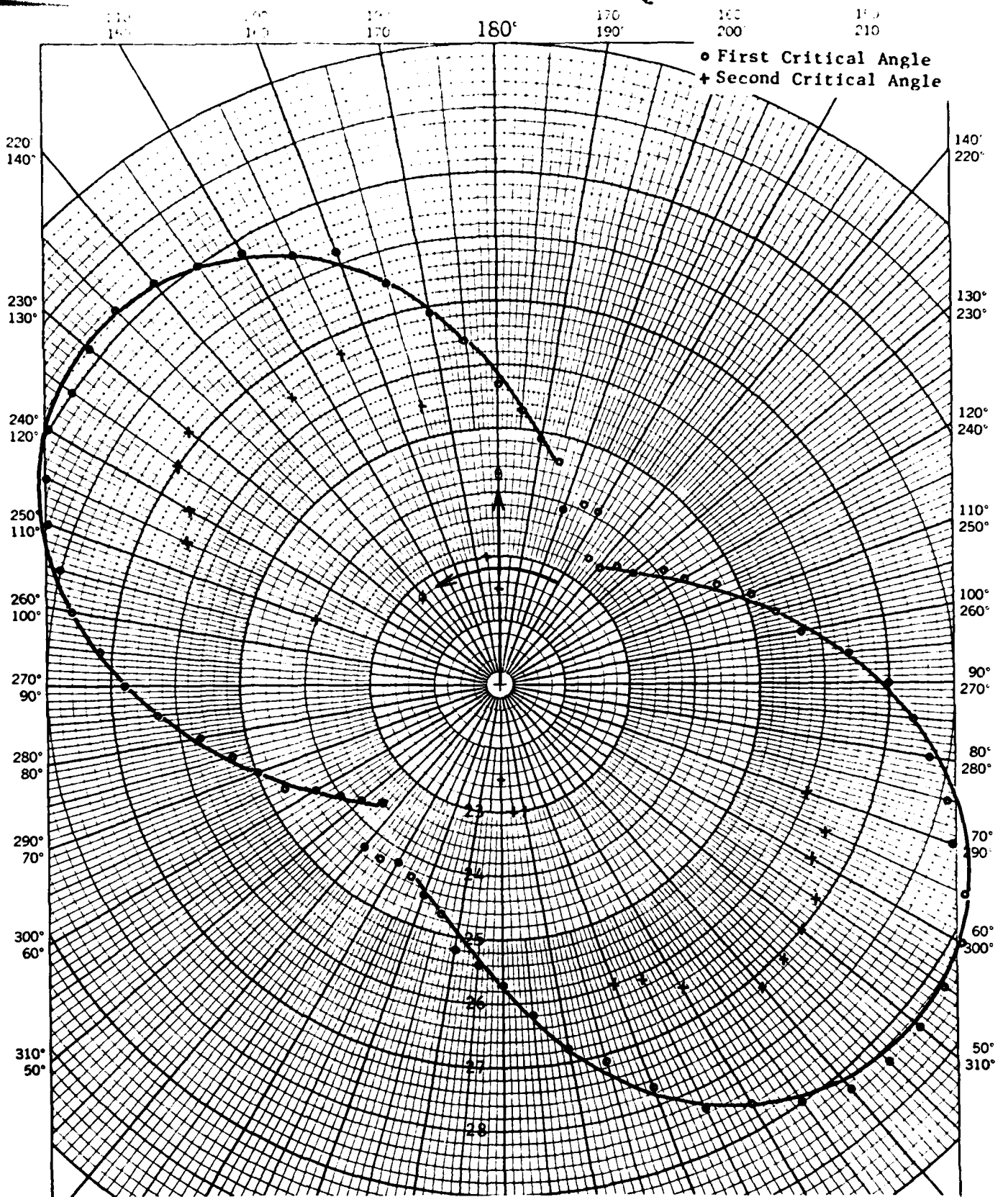


Fig. 5. Critical angles ( $\theta$ ) vs  $\phi$  for an x-cut quartz specimen. The frequency was 3.98 MHz, temperature 20°C, and source oscillator amplitude 6.5 volts. The axis of rotation was coincident with the x axis.

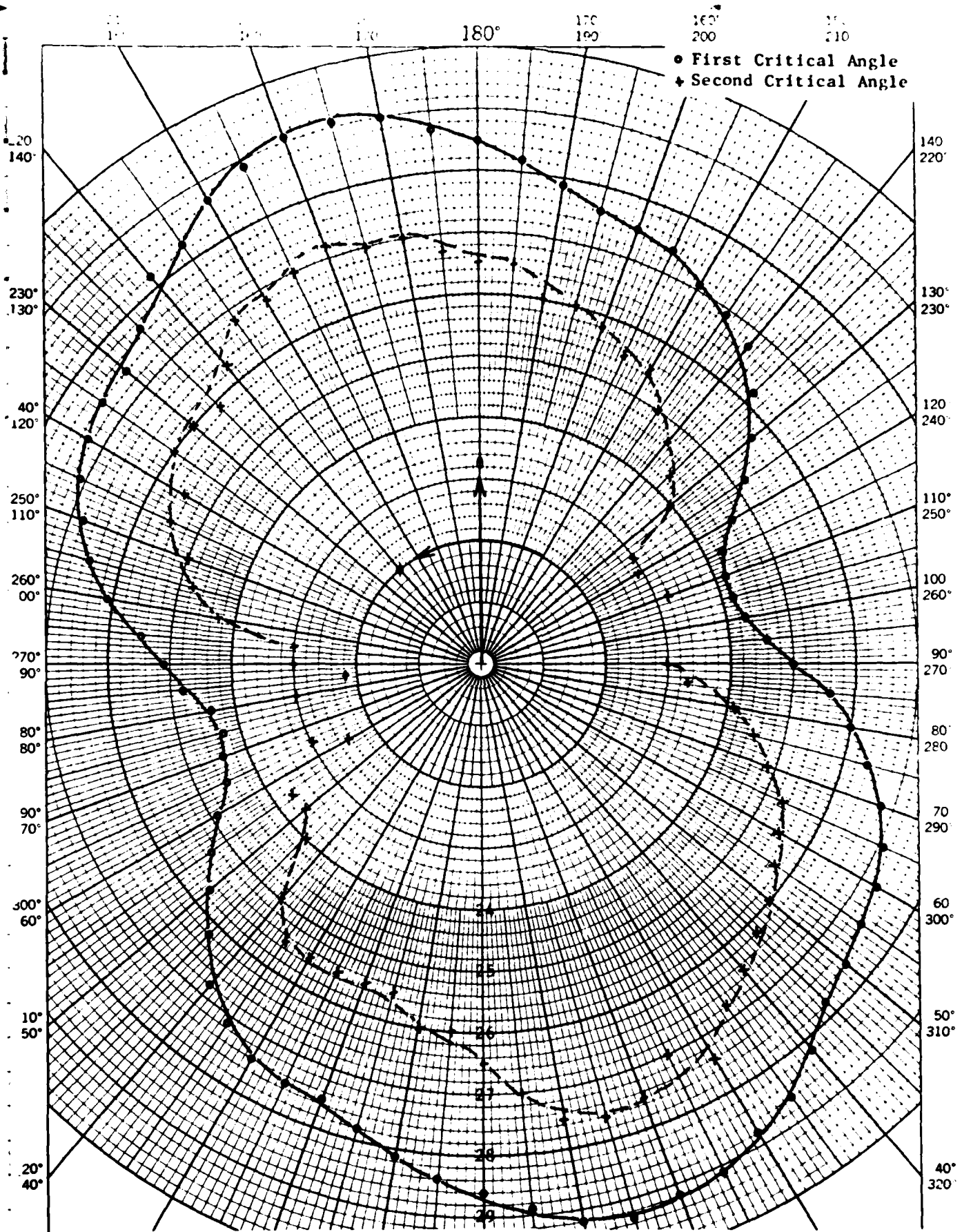


Fig. 6. Critical angles ( $\theta$ ) vs  $\phi$  for a y-cut quartz specimen. The frequency was 3.98 MHz, temperature 20°C, and source oscillator amplitude 6.5 volts. The axis of rotation was coincident with the y axis.

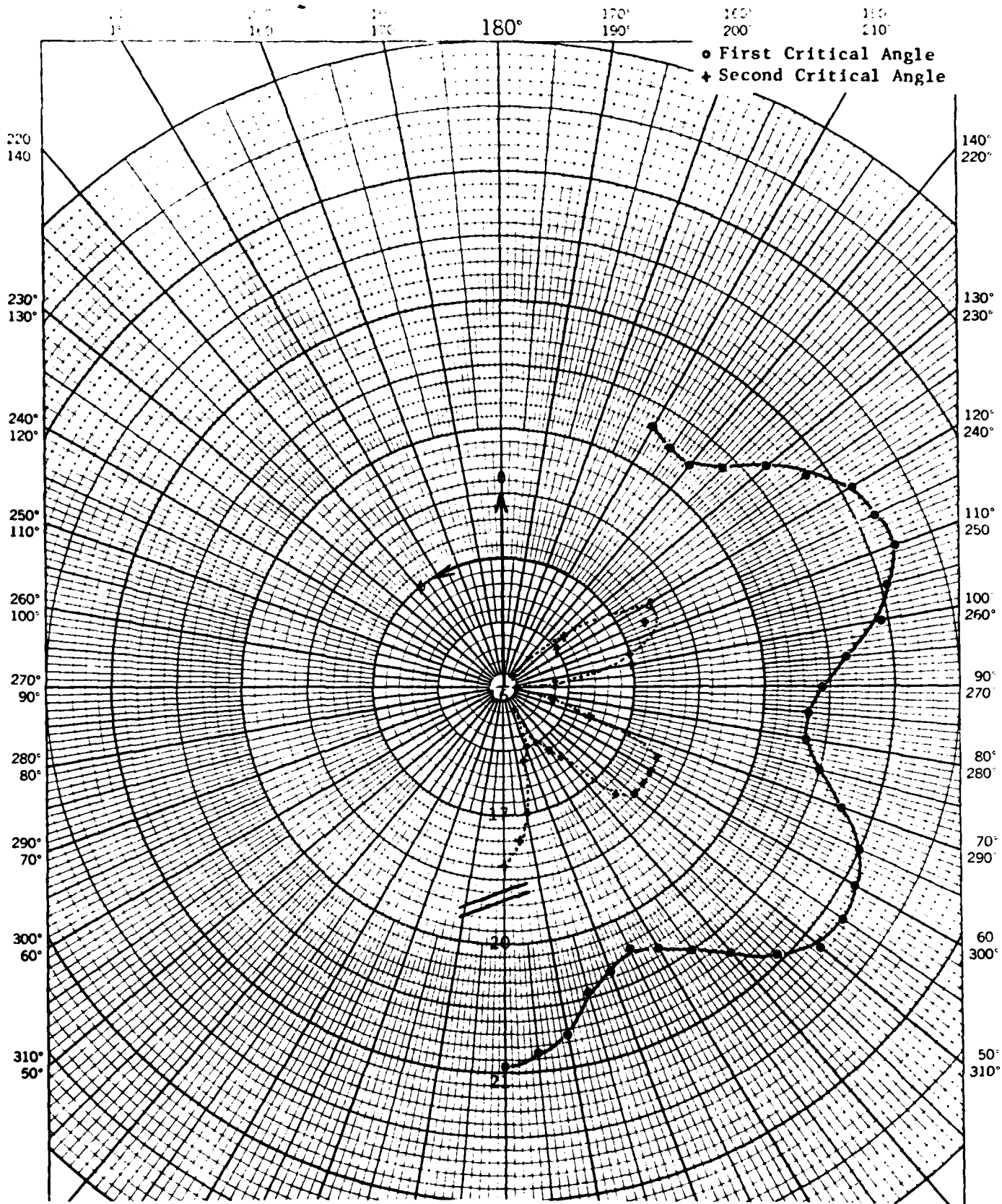


Fig. 7. Critical angles ( $\theta$ ) vs  $\phi$  for a silicon single crystal. The frequency was 6 MHz, temperature 20°C, and source oscillator amplitude 9 volts. This data is consistent with an axis of rotation coincident with the (111) axis of this cubic crystal.

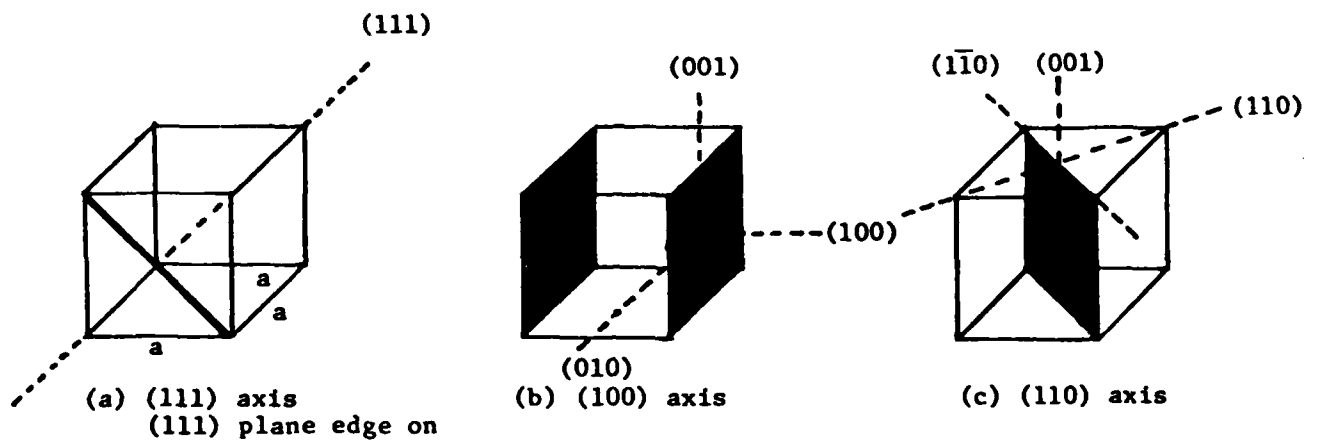


Fig. 8. Miller indices for cubic crystals. The axes are perpendicular to the shaded planes of the same designation. That is, the 100 axis is perpendicular to the 100 plane. Many directions are equivalent in a cubic crystal. For example, the 100 direction is equivalent to the 001 direction or the 010 direction in so far as bulk elastic properties are concerned.

angles showing the  $60^\circ$  periodicity (with  $\phi$ ) observed in Fig. 7. Thus, the axis of rotation was in fact the (111) axis and the silicon crystal has been oriented using critical angle measurements.

Not all crystals may be oriented, however, as illustrated by the measurements made on an aluminum single crystal. The crystal of aluminum, having a very low anisotropy parameter,<sup>8</sup> looks very nearly isotropic as illustrated by the critical angle measurements of Fig. 9. Clearly, such crystals cannot be oriented easily using critical angle measurements alone.

In Fig. 10 we illustrate the critical angle measurements on spinel ( $\text{Mg Al}_2 \text{O}_4$ ) which crystallizes in the cubic system. It is clear from these results that spinel has a very low anisotropy parameter. Like the aluminum crystal, critical angle measurements do not suffice to orient spinel. Anomalies (due to flaws or other defects) in the critical angle, observed in materials like spinel and aluminum are, therefore, unrelated to crystalline anisotropies.

Figure 11 illustrates the results obtained on lithium niobate which is a hexagonal crystal. However, our particular crystal was not oriented. These curves show a  $60^\circ$  periodicity (both critical angles) that is analogous to z-cut quartz (see September 30, 1982 Quarterly Report). Therefore, the axis of rotation we chose was the symmetry axis of the crystal. Again we have illustrated the capability of the measuring system to orient crystals.

Finally, in Fig. 12 we illustrate a series of measurements made on a titanium alloy with varying  $\text{O}_2$  content. One population of samples (two samples) with different but "low"  $\text{O}_2$  content (A and B) seem to have more or less isotropic characteristics. But, above a certain  $\text{O}_2$  content (samples C, D, and E) all of the samples appear to be anisotropic owing to the distinct elliptical patterns exhibited by curves of  $\theta$  vs  $\phi$  as in Fig. 12. Although the data is sketchy (more points on a given sample should be examined and averaged, for example), it does appear that a change in crystal structure has taken place above a threshold  $\text{O}_2$  content. In particular, below this threshold

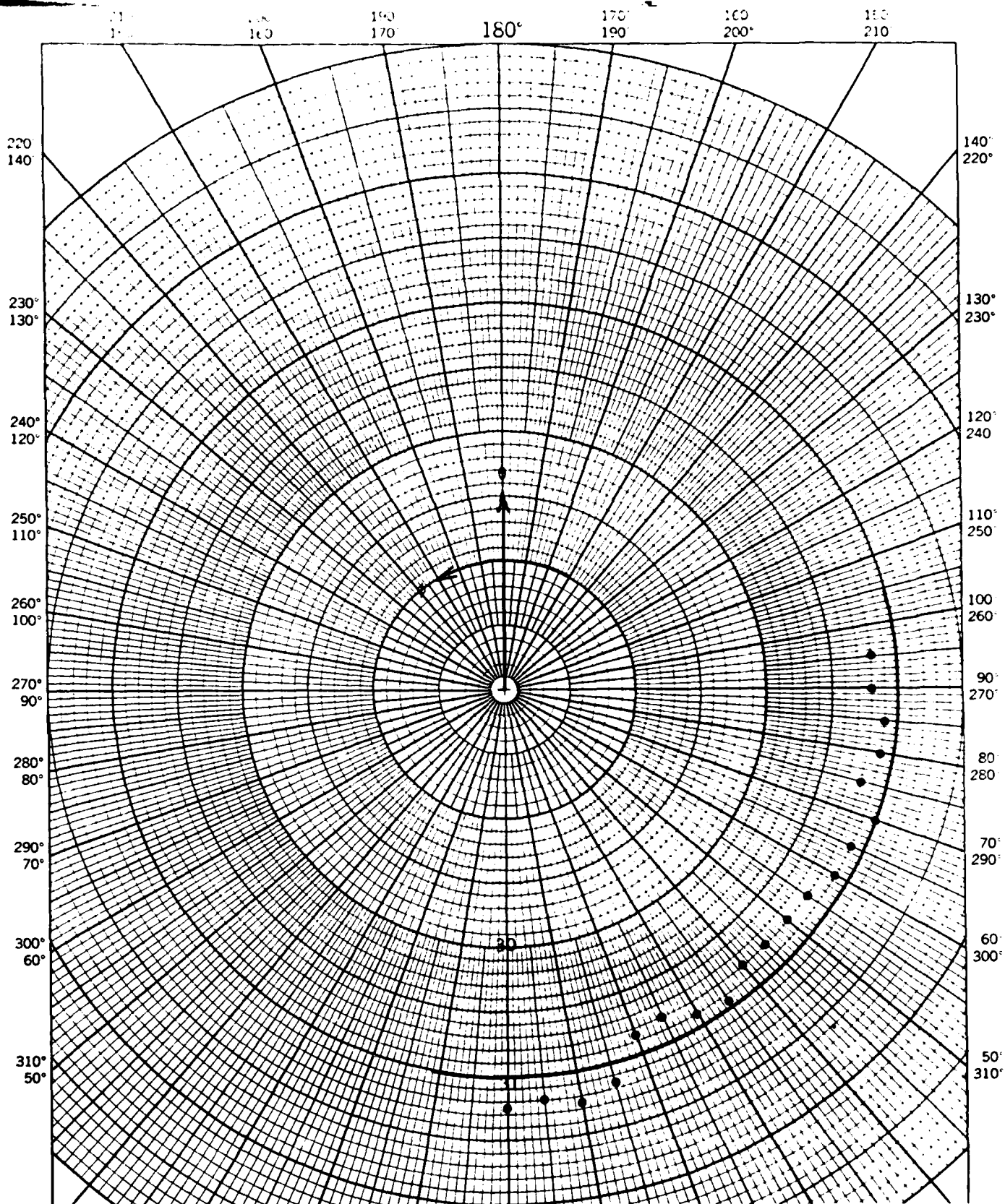


Fig. 9. Critical angles ( $\theta$ ) vs  $\phi$  for an aluminum single crystal. The frequency was 3.8 MHz, temperature 20°C, and source oscillator amplitude 9 volts. The axis of rotation was coincident with the (100) axis of this cubic crystal.



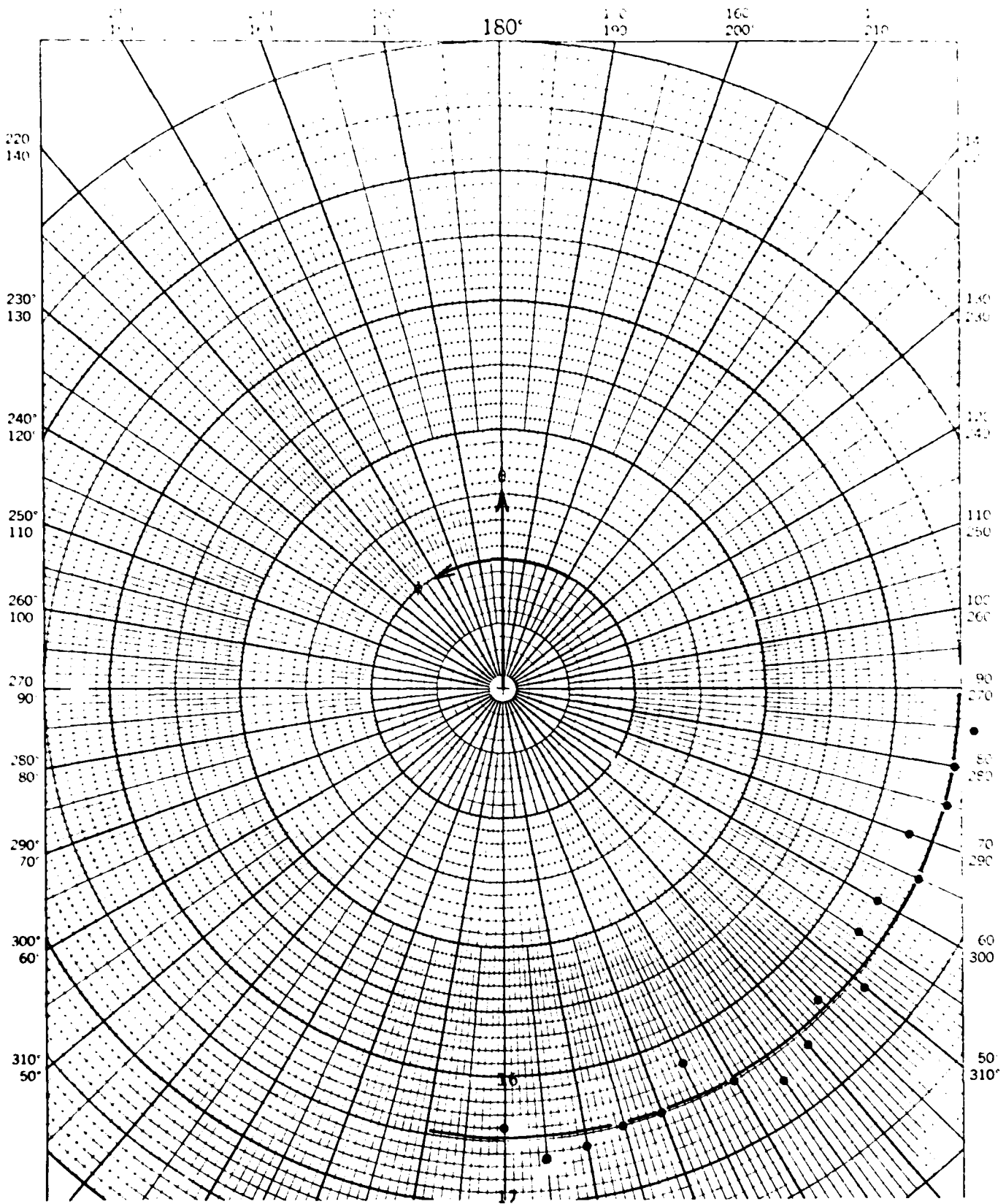


Fig. 10. Critical angles ( $\theta$ ) vs  $\phi$  for a spinel single crystal. The frequency was 4 MHz, temperature 20°C, and source oscillator amplitude 9 volts. The orientation of the axis of rotation with respect to the crystal axis is unknown.

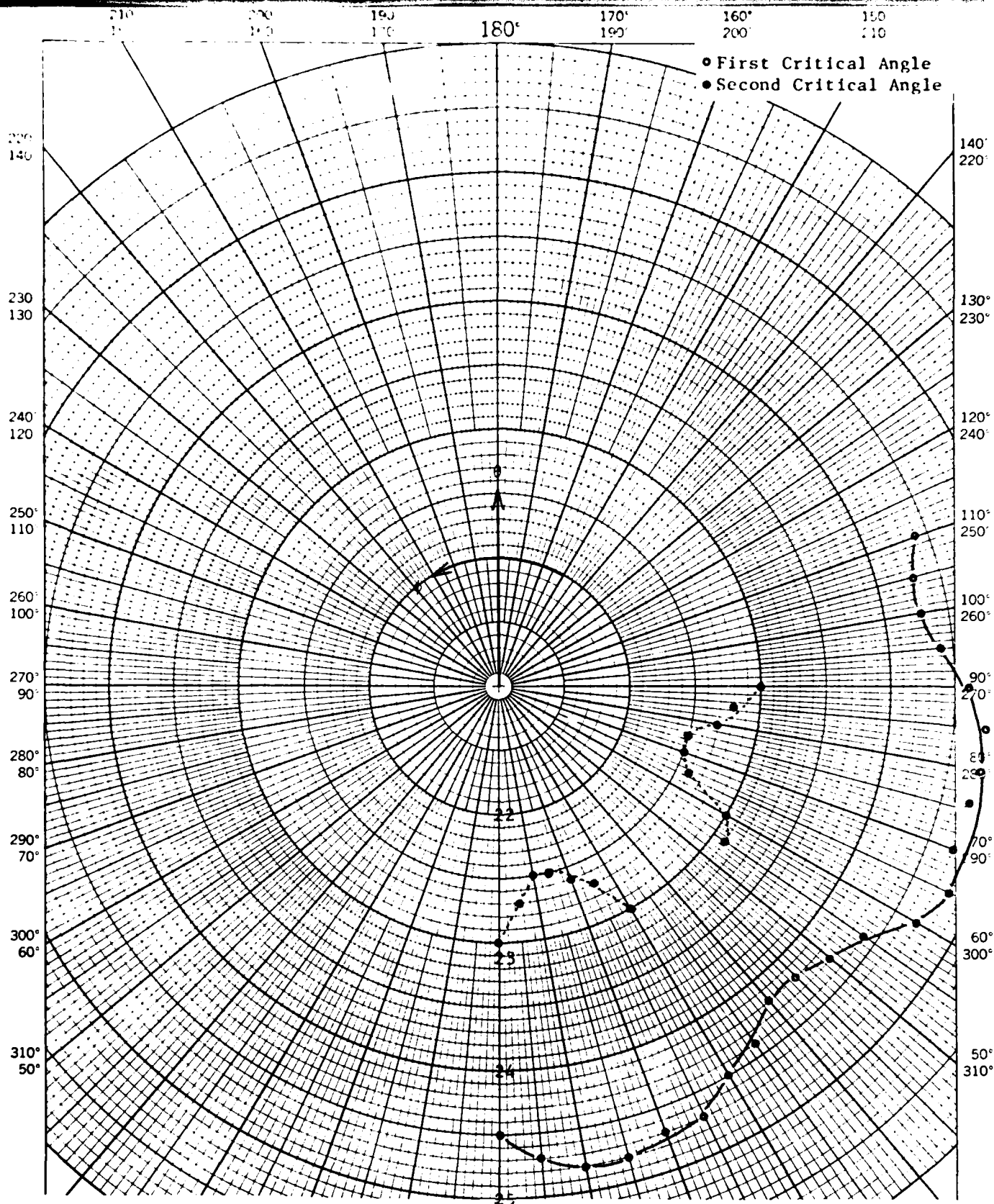


Fig. 11. Critical angles ( $\theta$ ) vs  $\phi$  for a single crystal of lithium niobate. The frequency was 4 MHz, temperature 20°C, and source oscillator amplitude 9 volts. The data are consistent with an axis of rotation coincident with the symmetry axis (c or z axis) of this hexagonal crystal.

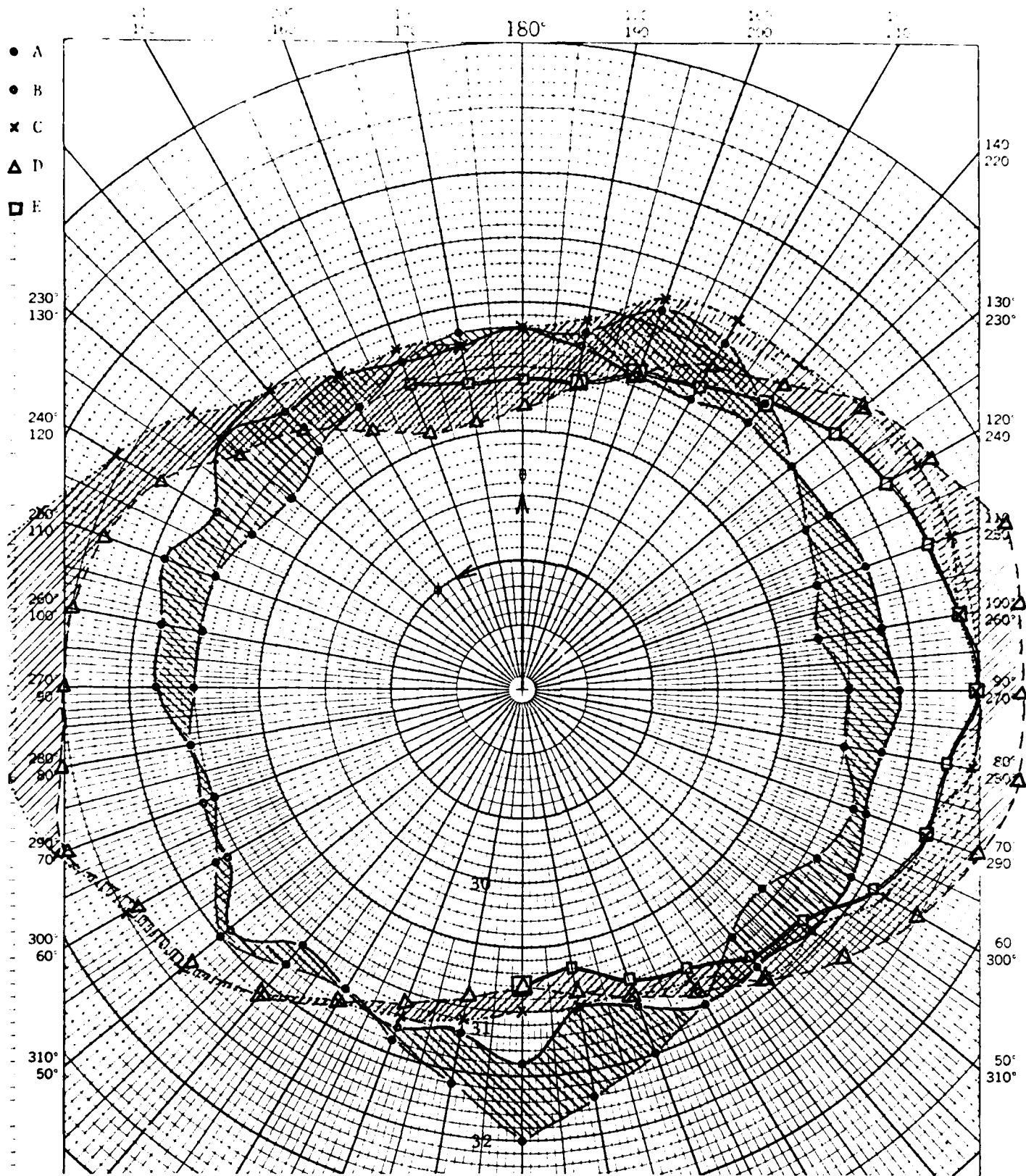


Fig. 12. This figure illustrates critical angle measurements on five specimens of a titanium alloy with varying  $O_2$  content. The  $O_2$  content increases from A to E. Curves for A and B seem to be more or less isotropic (circular pattern) while C,D,E fall in a distinctly elliptical pattern suggesting that a major crystalline anisotropy enters for specimens C,D,E. This change in crystal structure appears to occur at a certain threshold  $O_2$  content characteristic of specimen C.

the anisotropy parameter is small and above this threshold it is large. Although the detailed reasons for such behavior reside in the domain of metallurgy, it is clear that acoustic critical angle techniques might be helpful in characterizing or signaling the onset of such changes of the crystalline symmetry character of a specimen.

#### 4.0 SPECTRAL MEASUREMENTS

A dynamical physical system, such as the water path solid combination in our experiments, can be characterized by its frequency response. That is, the frequency spectra of the signals propagating through the system may be analyzed to determine the response of the system to various inputs. Any anomalies, such as nonlinearities, will then be characterized by changes in such spectra as a function of certain variables (source voltage, angle of incidence, etc). Although it is very difficult to obtain absolute spectral information in a complex electronic and physical system, owing to many coupled transfer coefficients, it is possible to obtain relative spectral information as certain quantities, such as incident angle  $\theta$ , are varied. During this quarter, we made improvements that allowed us to make such relative spectral measurements on nonspecularly reflected longitudinal waves (reflected and reradiated by leaky surface waves) at and near the Rayleigh critical angle. This information provides insights into the nature of the scattering process as a function of the angle of incidence ( $\theta$ ) of the longitudinal waves and other relevant variables.

##### Expanded Capabilities

We have expanded our experimental capabilities and are now able to measure

- (a) Amplitude
- (b) Phase
- (c) Mean Frequency

and (d) Frequency Spread (Standard Deviation)

of various individual reflected spectral lines (harmonics of a given fundamental frequency).

These tasks have been accomplished by a series of improvements to our hardware and software. We have programmed the IBM personal

computer so that it will calculate Fourier frequency spectra (using an FFT routine) from digitized time traces of the recorded signals (waves scattered from the test specimens). This operation, which provides the information needed to obtain a) through d) above, was formerly accomplished using the PDP 11/23 computer. Moreover, the 11/23 programs only provided information on a). The IBM now runs the entire critical angle measuring system which includes scanning of various types, data digitizing, and data analysis.

We have also constructed a high attenuation (-60DB) active filter to replace our earlier passive filter (-40DB). This new filter is capable of suppressing a fundamental at 3 MHz while passing second and higher harmonics with little effect. By using such a filter, one can examine higher harmonics in the absence of the large unwanted background signal at 3 MHz.

In addition we have recently upgraded our A-D board which is used to convert analog time signals to digital data for input into the Fourier spectral analysis programs. In its original form, this board was characterized by a digitizing rate of 20 MHz which meant that the highest frequency that could be digitized and recorded was about 10 MHz. When examining signals with a fundamental frequency of 3 MHz, this requirement means that we could only expect to observe higher harmonics up to the third ( $\approx 9$  MHz). With the upgraded board, we can now digitize at a rate of 50 MHz which means that harmonics up to the 8th can be measured for an input fundamental of 3 MHz.

Software that allows us to measure the phase, mean frequency, and standard deviation of a given reflected spectral line has also been implemented.

We are in the process of making such spectral measurements on samples ranging from glass to various single crystals. These measurements involve examining spectra as a function of

1) Incident angle  $\theta$

2) Input amplitude

and 3) Sample orientation  $\phi$

among other variables.

In Fig. 13 we illustrate measured amplitudes of the first and second harmonics (the third harmonic amplitude was too noisy) observed to be present in the received scattered signal from a specimen of optical glass as  $\theta$  is varied. Because glass is isotropic, the observed increase in the second harmonic as the critical angle is approached is clearly unrelated to anisotropy. It is suggested that such effects are the result of nonlinearities in the solid.

Standing in the way of a better understanding of such effects is the absence of absolute spectral measurements. We believe that absolute measurements of amplitudes, mean frequency, standard deviation and phase of various spectral lines scattered from a target, at and near the critical angle, will provide significant constraints on the complete physical description of the critical angle phenomenon. Accordingly, we will continue to improve our capability to make such measurements.

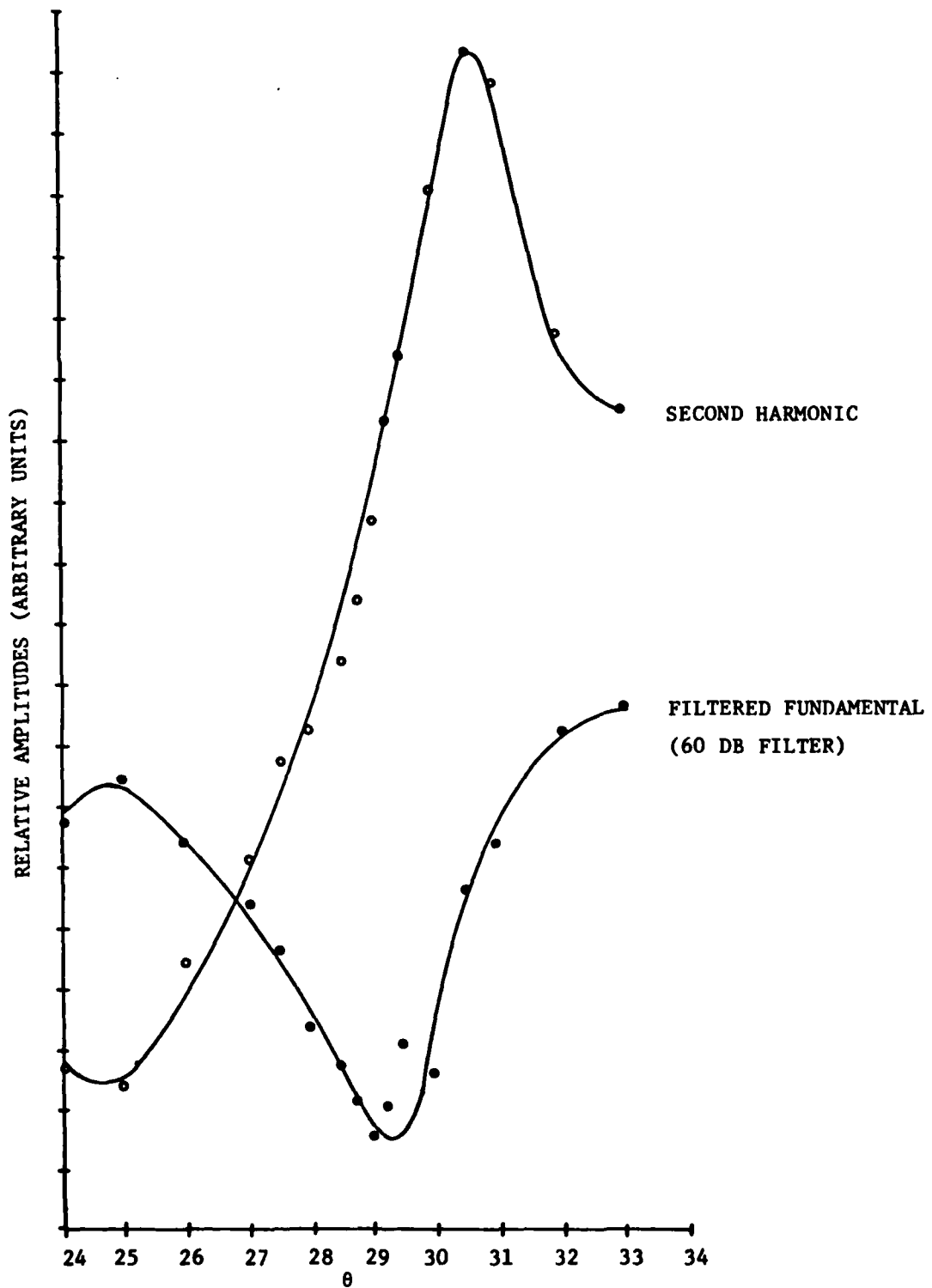


Fig. 13. This figure illustrates fundamental and second harmonic amplitudes present in the reflected signal from an isotropic specimen of optical glass at and near the Rayleigh critical angle. Note the drop in amplitude of the fundamental at  $\theta_c$  and the increase in the second harmonic at the same angle. The anomalous production of such higher harmonics suggests that nonlinearities are important at the critical angle.



## 5.0 SUMMARY

We have performed numerous critical angle experiments on a variety of samples ranging from single crystals to polycrystalline alloys and glasses. Two basic conclusions can be drawn from this work: 1) simple linear equations of motion (which include anisotropy) suffice for an approximate description of the observations (for example, the value of various critical angles can be calculated from a knowledge of second order elastic constants alone); 2) certain observations at and near the critical angle, involving the production of anomalous harmonics, strongly imply that the nonlinear characteristics of the solid (third order elastic constants) cannot be ignored.

Nevertheless, there are still other possible explanations for these effects involving the nonlinear properties of water. Accordingly, further spectral response measurements of a more absolute nature are being pursued. Such measurements should provide a complete characterization of the phenomenon including the separate roles played by the water path and the solid.

## 6.0 ACKNOWLEDGMENTS

The authors thank R. Silta for performing experiments, drafting, and construction of experimental apparatus. We also thank Y. Pipkin for editing and typing the manuscript, and T. Davis for designing the line suppression filter used in our spectral measurements.

## 7.0 REFERENCES

1. L. D. Landau and E. M. Lifshitz, Theory of Elasticity, Vol. 7, Pergamon Press, New York (1975).
2. G. W. Farnell, "Properties of Elastic Surface Waves," Physical Acoustics, Vol. VI, edited by W. P. Mason, Academic Press, New York (1970).
3. M. A. Breazeale, "Ultrasonic Studies of the Nonlinear Properties of Solids," Intl. J. NDT 4, 149-166 (1972).
4. B. P. Hildebrand and G. L. Fitzpatrick, "Investigation of the Rayleigh Critical Angle Phenomenon for the Characterization of Surface Properties, Phase I," Fifth Quarterly Technical Report for AFOSR (June 1982).
5. Igor Aleksandrovich Viktorov, Rayleigh and Lamb Waves, Plenum Press, New York (1967).
6. Thomas J. Plona et al., "Ultrasonic Bounded Beam Reflection Effects a Liquid-Anisotropic-Solid Interface," J. Acoust. Soc. Am. 56, 1773 (1974).
7. F. L. Becker and R. L. Richardson, "Ultrasonic Critical Angle Reflectivity," Research Techniques in Nondestructive Testing, edited by R. S. Sharpe, Academic Press, London, 91-130 (1970).
8. Landolt-Börnstein, Numerical Data and Functional Relationships in Science and Technology, Vol. 2, edited by K. H. Hellwege and A. M. Hellwege, Springer-Verlag, New York (1969).